

Research Article

Dynamic RCS Reduction Performances of Antenna Array with Coding Metasurface

Yan Chen, Xiao-Xiang He, Yang Yang , Heng-Yan Hu, Fu-Kang Li, and Lei Yang

College of Electronic and Information Engineering, Nanjing University of Aeronautics and Astronautics, Nanjing, China

Correspondence should be addressed to Yang Yang; eeyy@nuaa.edu.cn

Received 16 August 2021; Revised 16 February 2022; Accepted 24 February 2022; Published 14 March 2022

Academic Editor: Atsushi Mase

Copyright © 2022 Yan Chen et al. This is an open access article distributed under the Creative Commons Attribution License, which permits unrestricted use, distribution, and reproduction in any medium, provided the original work is properly cited.

On the basis of combining the two concepts of digital coding metasurface and metasurface antenna, low radar cross-section (RCS) coding metasurface antenna array with dynamic scattering performances is presented in this paper. Extending scattering factor theory to coding metasurface antenna, by controlling the states of PIN diodes randomly, the scattering performances of coding metasurface antenna array can be tuned dynamically without degrading its radiation property. Based on phase cancellation principle, a 8×8 antenna array was finally simulated and fabricated. By comparing several different layouts, taking checkerboard layout, new chessboard layout, and “0101” square ring nested layout as examples, both monostatic and bistatic RCS of the antenna mentioned above can be reduced 10 dB or more in the frequency range of 9–10.5 GHz under the illumination of x-polarized incident wave. The measured data are consistent with the simulation data, which proves the effectiveness of the proposed method.

1. Introduction

As a special strong scatter, the reduction of antenna radar cross section (RCS) plays a crucial role in improving the survival and competitiveness of all kinds of weapons. It is hard to ensure the normal radiation performance of the antenna only adopting traditional methods of reducing RCS. A large sea of works have been put forward to solve this tough task. Based on the analysis of the comparison between the radiation and scattering current distribution on the metal patch, antenna shape stealth technology came into being [1, 2]. The principle of this method is finding out the area where current distribution is sparse, by modifying the configuration of this area; the scattering property of the antenna can be controlled effectively while maintaining its satisfactory radiation performance. For military platforms, one of the most useful means is loading frequency selective surface (FSS) [3–5]. FSS radome is usually used as a filter to control the electromagnetic scattering of the aircraft head, which is a solution to realize out-band antenna stealth. Also, by means of coating absorbing materials, the incident

electromagnetic wave can be dissipated [6, 7], so as to realize the stealth effect. Recently, metasurfaces have attracted worldwide attention. Due to their extraordinary ability to control electromagnetic waves, some types of them have been utilized to reduce RCS of target, such as artificial magnetic conductor (AMC) [8], polarization conversion metasurface (PCM) [9], metamaterial absorber (MA) [10, 11], and digital coding metasurface [12–17]. However, most of these applications of metasurfaces are not combined with the antennas, or they are designed separately. This not only increases the complexity of the design process but also the relatively higher profile of the overall structure is not good for the actual fabrication and application.

In order to solve the aforementioned problem, metasurface antenna has been proposed to satisfy the needs of the integrated design of metasurface and antenna [18–23]. As is proposed in [22], the unit of 2×2 SRRs array can not only be regarded as a liner polarized antenna element but also be considered as the metasurface cell. For scattering property, these elements are designed to have a 180 degree reflective phase. Then, by arranging them into checkerboard layout,

the ideal RCS reduction effect can be achieved. For radiation performance, due to the antenna array is fed with phase shift of 90 degrees and positioned in an orthogonal direction, it possesses left-handed circular polarization property. This method is further improved in [23] by using two different antenna elements which can meet the requirement of 180-degree reflection phase difference and approximately same radiation property simultaneously in a 4×4 array. Broadband RCS reduction can then be obtained while the total gain is almost not unaffected. In order to find the optimal solution, two kinds of antenna super arrays with the same upper layer patch shape and different feeding structure are designed. The optimal arrangement of the super array with the lowest RCS peak can be calculated using genetic algorithm. However, these structures inevitably have a common problem. Once the design is completed, the radiation performance and scattering property of the antenna are fixed, so they can only be applied to single engineering system. In order to make the antenna system applicable for changeable and complex battlefield situation in the future, it is urgent to design a suitable antenna with its scattering pattern which can be tuned real time.

In this paper, to address this matter, a 1 bit low RCS coding metasurface antenna array with dynamic scattering performances is presented. A parasitic square ring which has little effect on the radiation performance of the antenna array is loaded around the rectangular patch and PIN diodes are embedded onto the metasurface as active components. By changing the "ON" and "OFF" states of PIN diodes real time, different types of scattering patterns of the metal layer can then be obtained. Furthermore, the overall RCS of the antenna array is reduced to meet the requirement of antenna stealth. The rest of this paper is as follows: Section 2 describes the theoretical analysis and design procedure of 1 bit coding metasurface antenna array. Section 3 shows the simulation and experimental results of this antenna to demonstrate the feasibility of this method, and finally, Section 4 is the summary of this work.

2. Theoretical Analysis and Design Procedure

2.1. Scattering Mechanism of Coding Metasurface Antenna. To clearly explain the physical mechanism of RCS reduction, here the method of analyzing scattering factor [23] of planar antenna array is adopted. Assuming that the scattering field of unit cell remains same ignoring the coupling effect of adjacent antenna elements, theoretically the total RCS of the antenna array can then be obtained by multiplying the element scattering factor by the array factor:

$$\sigma(\theta, \varphi) = \sigma_e(\theta, \varphi) \cdot \sigma_a(\theta, \varphi), \quad (1)$$

where σ_e represents the unit scattering factor and σ_a represents array factor. Considering the $m \times n$ scale antenna array shown in Figure 1, the element spacing of x -direction and y -direction is dx and dy , respectively, and the phase mutation introduced by the unit in the m th row and n th column is δ_{mn} , and corresponding scattering factor can be expressed as [24]

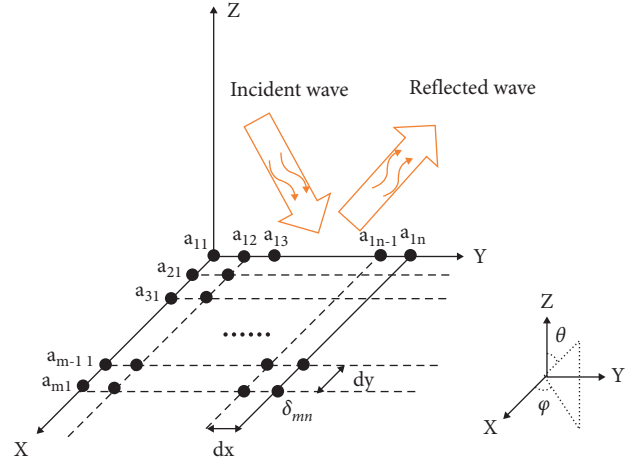


FIGURE 1: Schematic diagram of antenna array.

$$\delta_{mn} = k(m dx \cos \varphi + n dy \sin \varphi) \cdot \sin \theta, \quad (2)$$

$$\begin{aligned} \sigma_{tot}(\theta, \varphi) &= \sum_{p=1}^{p=m} \sum_{q=1}^{q=n} e^{j[k(m dx \cos \varphi + n dy \sin \varphi) \sin \theta]}, \\ &= \sum_{p=1}^{p=m} \sum_{q=1}^{q=n} e^{j\delta_{mn}}. \end{aligned} \quad (3)$$

Extending aforementioned principle to coding metasurface antenna, when all pin diodes are of "ON" states (namely, "1" element), scattering factor can be calculated as equation (3) similarly, while all pin diodes are of "OFF" states (namely, "0" element); total scattering factor expression is as follows:

$$\begin{aligned} \sigma_{tot}(\theta, \varphi) &= \sum_{p=1}^{p=m} \sum_{q=1}^{q=n} e^{j[k(m dx \cos \varphi + n dy \sin \varphi) \sin \theta] + \pi}, \\ &= \sum_{p=1}^{p=m} \sum_{q=1}^{q=n} e^{j(\delta_{mn} + \pi)}. \end{aligned} \quad (4)$$

Therefore, when the plane wave is incident perpendicularly, by controlling the reflection amplitude of each unit keeping same, the two-dimensional scattering factor of coding metasurface antenna can then be calculated as

$$\begin{aligned} \sigma_{tot}(\theta, \varphi) &= \sum_{p=1}^{p=m} \sum_{q=1}^{q=n} e^{(j[k(m dx \cos \varphi + n dy \sin \varphi) \sin \theta] + \Gamma_{mn} \pi)}, \\ &= \sum_{p=1}^{p=m} \sum_{q=1}^{q=n} e^{j(\delta_{mn} + \Gamma_{mn} \pi)}, \end{aligned} \quad (5)$$

where Γ_{mn} is a variable, it represents when all pin diodes of the unit in the m th row and n th column are of "ON" states, the value of Γ_{mn} is 0, conversely when all pin diodes are of "OFF" states, and Γ_{mn} equals to 1. So, it can be concluded that due to the uncertainty of unknown Γ_{mn} , the two-dimensional checkerboard arrangement or other different layouts of coding metasurface antenna units with various

scattering factors can produce scattering zero points in the traditional reflection direction.

2.2. Design of Coding Metasurface Antenna. As is shown in Figure 2(a), this multilayer structure is divided into three parts: the phase-controlled metal patch layer, the feeding network layer, and the bottom direct current (DC) bias line layer used to provide voltage to diodes. First step is the design of the metal patch layer. A simple rectangle patch antenna is designed according to the microstrip patch antenna design theory. The geometry of proposed metasurface antenna is listed in Figure 2(b). Two PIN diodes are mounted in the slots of the parasitic square ring and other two pin diodes are placed in the gaps to provide a connection of square ring and patch. The type of selected PIN diodes is MACOM MADP-000907-14020. When these PIN diodes are of “ON” states, they can be modeled as a series circuit of a resistor (7.8 Ω) and an inductor (30 pH). While they are in “OFF” states, they can be seen as a series circuit comprising a capacitor (20 fF) and an inductor (30 pH). In order to avoid the influence of the antenna array feeding network on the antenna RCS, a corresponding Wilkinson power divider is designed to be connected to the upper patch layer through coaxial metal columns, as in Figure 2(c). They are connected to the negative pole of the power supply. Figure 2(d) is the side view of whole structure. Finally, optimized DC power lines are etched on the bottom layer of whole structure to power upper PIN diodes. They are connected to the upper parasitic square ring through green metal column as in Figure 2(e) to provide positive current. The four PIN diodes in a unit are powered together. Sixty-four metal patches are arranged under the 8×8 metasurface antenna array periodically, which is convenient for random control of the ON-OFF states of unit independently. For the antenna unit structure in Figure 2(b), the unit cell boundaries are set in the x - and y -directions, while open (add space) boundaries are set in the z direction. In addition, the Floquet port excitation is set as wave source. In order to verify the influence of loading parasitic unit and active components to coding metasurface antenna, we need to conduct preliminary analysis on the surface current of the antenna array. Figures 3(a) and 3(c) are the comparison of radiation current distribution on the surface of antenna when all the pin diodes are on and off. It can be seen from the figures that the area having the strongest current (which is the red area) is the wide edge of rectangular patch. The current on the parasitic rectangular ring is almost dark blue, which means that current here is weakest. So, we can verify that the loading of the parasitic element does not affect the radiation performance of the original patch antenna. Figures 3(b) and 3(d) are the comparison of scattering current distribution on the surface of antenna. The difference from the radiation situation is that the side region of parasitic rectangular ring which is close to rectangular patch is also current-dense area in addition to the patch itself. Furthermore, through the analysis of the scattering states, we can see that when pin diodes are powered off, only the lower half of parasitic rectangular ring has a denser current distribution; when they

are powered on, both the upper and lower halves of parasitic rectangular ring have strong current distribution due to connection of pin diodes that verifies by means of loading PIN diodes on slotted square ring to change the length of current flowing path while maintaining radiation pattern is practical. According to the principle of equivalent circuit, the metal patch can be equivalent to inductor, the interval between two adjacent patches can be equivalent to capacitor, and the diode itself can be equivalent to an RLC series circuit. By optimizing size of the parasitic rectangular ring and selecting appropriate diodes, the required phase difference can be realized due to the difference of the current flowing path. Finally, we choose F4B material (with relative dielectric constant 2.65, and loss tangent 0.001) as all dielectric substrates.

3. Simulation and Measured Results of Coding Metasurface Antenna

3.1. Simulated Results of Antenna Unit. The full-wave simulation results are carried out using CST commercial software. For the overall structure of the 8×8 coding metasurface antenna array, free space is set as boundary condition. At the same time, in this journal, in order to simulate the far-field scattering characteristics of antenna, plane wave excitation method is adopted and 50Ω terminal matching method is used for all antenna ports. In Figure 4(a), the bandwidth $|\varphi_1 - \varphi_2| = 180^\circ \pm 37^\circ$ is observed within 9.5 to 10 GHz. The nearly same resonant frequency point and radiation performance can be gotten from Figures 4(b)–4(c). When four PIN diodes are of “OFF” states, the simulated gain of coding metasurface antenna unit is 7 dB; when four PIN diodes are of “ON” states, the simulated gain is 6.1 dB.

3.2. Comparison of Different Layouts. Letting all the active components of antenna array of “ON” or “OFF” states cannot achieve the effect of reducing RCS. Only when two antenna units (“0” and “1” element) with different scattering factors are arranged randomly in two-dimensional antenna array, effective scattering zero point can be obtained in the traditional reflection direction. In order to express different layouts more clearly and intuitively, here we use the yellow lattices to replace the “OFF” state (namely, “0” element) while green lattices represent “ON” state (namely, “1” element). Figure 5 depicts several different layouts, taking checkerboard layout, new chessboard layout, and “0101” square ring nested layout as example.

To verify the feasibility of coding metasurface antenna array, a 8×8 square coding metasurface composed of two designed elements is finally built. The radiation and scattering performance comparison of different layouts of antenna array is conducted. Figure 6 shows that by controlling voltage provided for PIN diodes, dynamic scattering patterns can be obtained. Figure 6(a) is the three-dimensional scattering diagram of reference antenna under the illumination of cross-polarized wave. It can be obviously seen that a main peak beam exists in the traditional mirror reflection

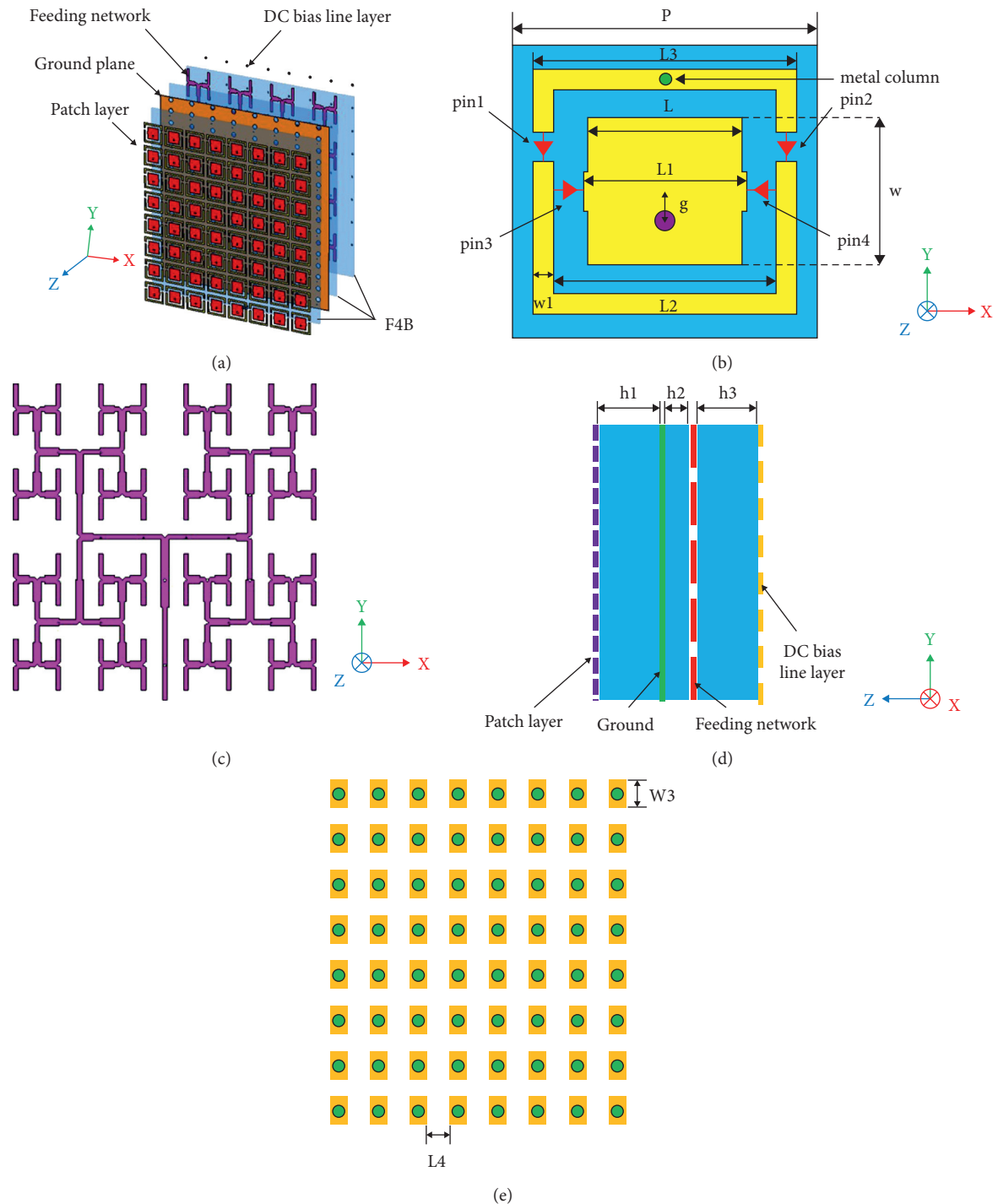


FIGURE 2: (a). Overall view of whole structure; (b) dimensions of proposed metasurface antenna unit including $p = 15$ mm, $g = 1.5$ mm, $L = 7.6$ mm, $L_1 = 8$ mm, $L_2 = 11$ mm, $L_3 = 13$ mm, and $W = 7.5$ mm; (c) overall view of feeding network; (d) side view of whole structure where $h_1 = h_3 = 1.6$ mm, $h_2 = 0.6$ mm; (e) overview of DC power lines where $W_3 = 1$ mm, $L_4 = 14.4$ mm.

direction, and Figure 6(b) is the scattering pattern of checkerboard layout. We can see original main scattered beam is suppressed and points to four quadrants. Figure 6(c) explains the scattering situation of new chessboard layout. As we can see that the main peak beam is dispersed into four areas according to the divided triangular region, and next Figure 6(d) is the scattering performance of a nested layout

of square rings in the sequence of "0101," like the theoretical prediction, a corresponding null will be generated at the junction of "0" and "1" unit cells. Figure 6(e) is monostatic RCS variation curve with frequency; it can be obviously concluded that certain reduction of radar cross-section can be achieved no matter which layout the coding metasurface antenna is of, especially when it is in checkerboard layout

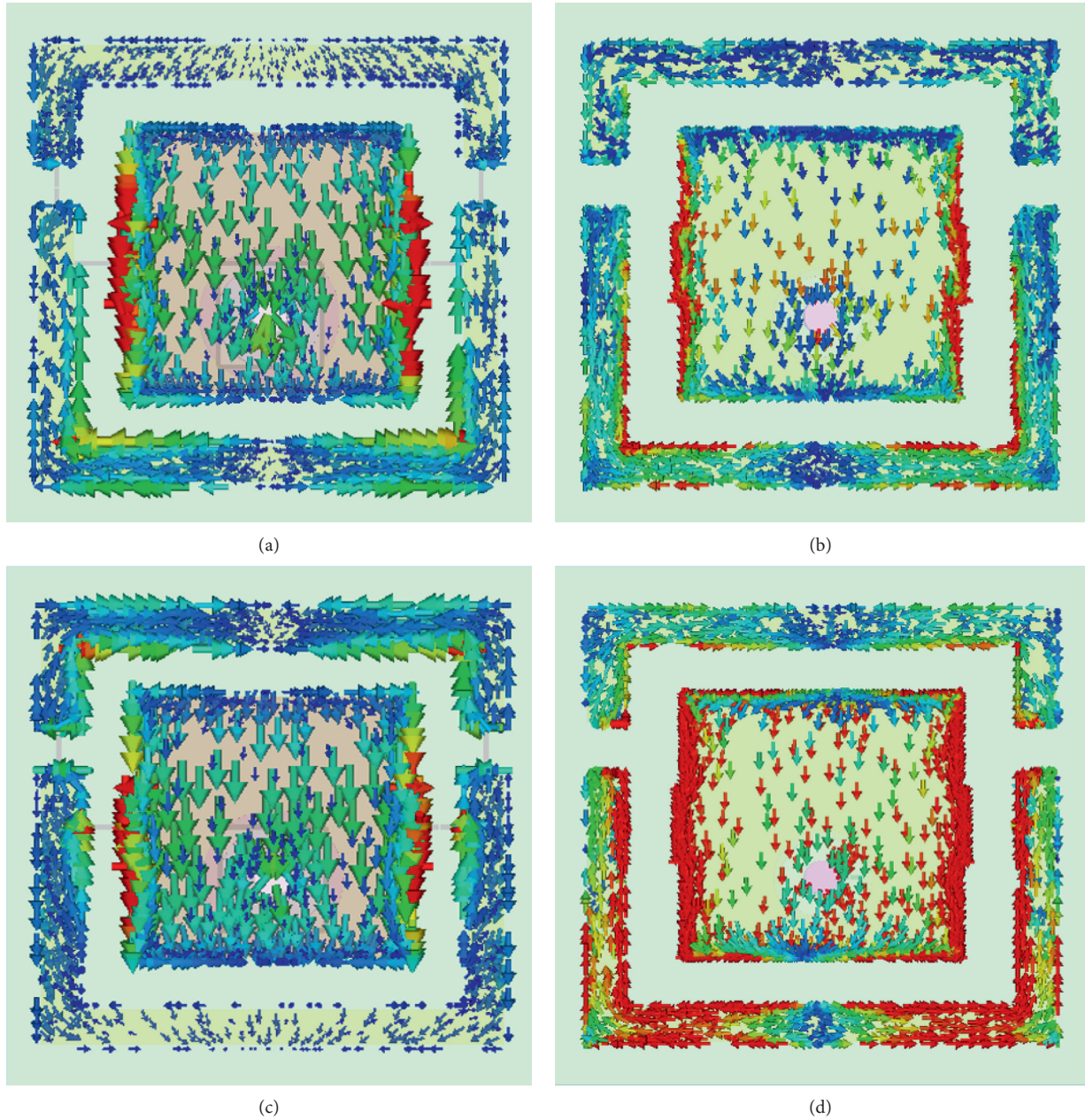


FIGURE 3: Surface current analysis; (a) surface current distribution on radiation state (“OFF” state); (b) surface current distribution on scattering state (“OFF” state); (c) surface current distribution on radiation state (“ON” state); (d) surface current distribution on scattering state (“ON” state).

within the frequency range of 9.0–10.5 GHz. According to Figure 6(f), bistatic RCS changing curve with angle, the RCS of antenna can realize a reduction of more than 10 dB compared with reference antenna in the range of $-60^\circ \sim 60^\circ$ at 9.5 GHz when they are arranged as Figure 5(b).

From the antenna radiation property point of view, the antenna works at 9.0–9.5 GHz and 10.2–10.6 GHz. Compared to two reference antennas, the resonant frequency band of coding metasurface antenna array is basically unaffected. When all PIN diodes are of “ON” states, the gain at two working frequency bands is 15.9 dB and 19.3 dB, respectively, while all PIN diodes are of “OFF” states, the gain

at two working frequency bands is 18.9 dB and 21 dB separately. Then, when antenna exhibits dynamic scattering performance, just take most common checkerboard layout as an example; the gain at two resonance frequency points is 18.1 dB and 20 dB, as shown in Figures 7 and 8. It can be concluded that the presented antenna array can realize effective RCS reduction in the condition of radiation performance nearly consistent with reference antennas.

According to the theory, for $N \times M$ metasurface antenna arrays which are composed of 1-bit coding units, the controllable number of states can be up to $2NM$. Therefore, the 8×8 coding metasurface antenna array studied in this

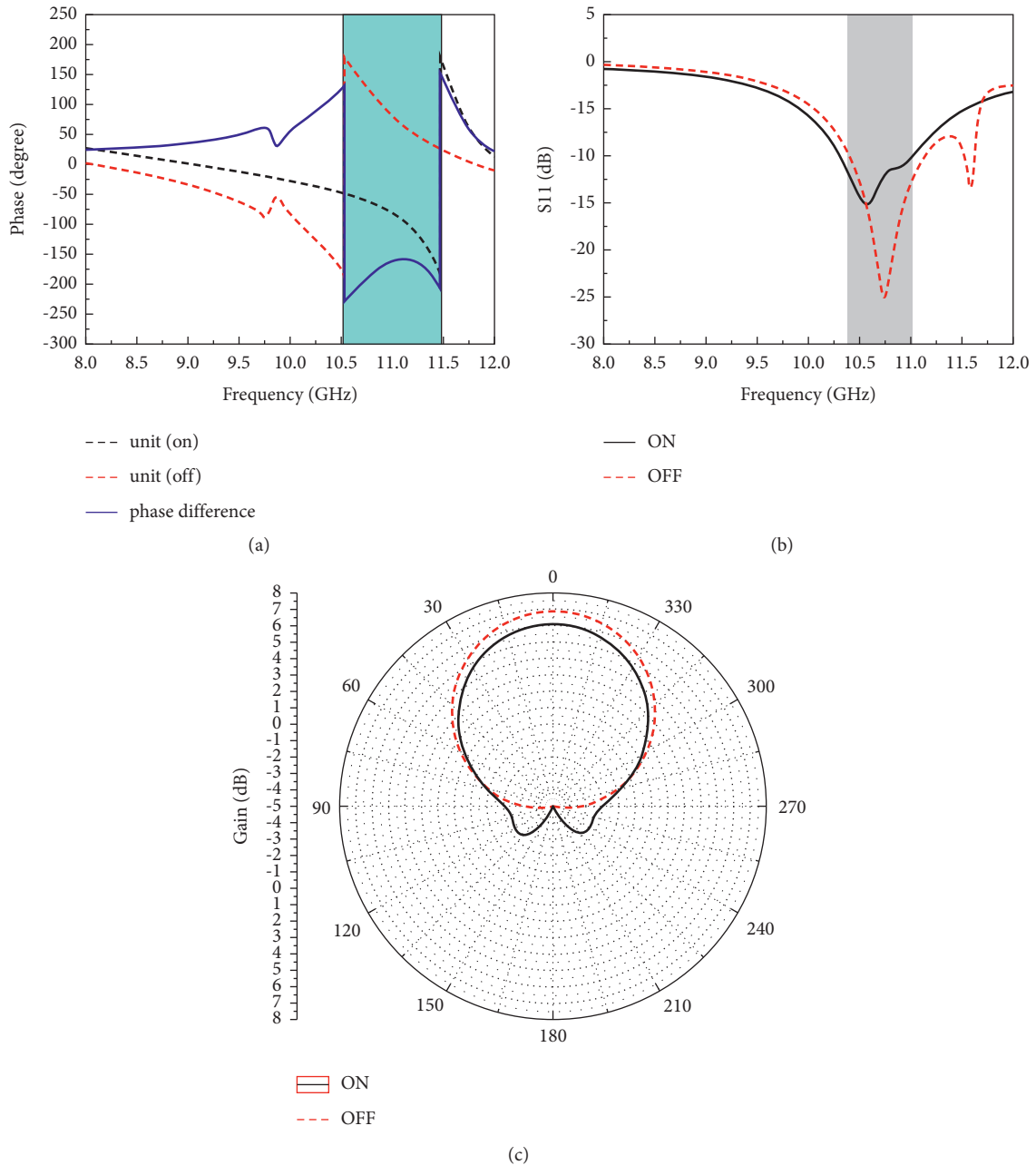


FIGURE 4: Simulated results of proposed antenna unit; (a) phase information of "ON" and "OFF" states; (b) amplitude of reflection of two states; (c) simulated gain of two states.

journal has 128 controlled states theoretically. Excluding repeated scattering patterns and all ON/OFF states, the actual agility degrees of freedom of scattering states will be less than 128. But in general, the designed antenna can display the "fake" RCS effect while achieving stealth purpose. This shows advantage of dynamically adjusting RCS reduction. By improving the degree of freedom of antenna's scattering agility, it can not only achieve the RCS reduction effect but also deceive and confuse enemy to a certain extent. The basic performance comparison of three different layout antennas and reference antenna are given in Table 1.

3.3. Fabrication and Measurements. In order to further validate the practicality of the proposed antenna array, a 8×8 prototype was finally fabricated and corresponding measured dates were recorded by using anechoic chamber. The photos of fabricated antenna and testing environment are shown in Figure 9(a). Here, just taking checkerboard layout as an example, the measured scattering and radiation performances of antenna are as follows: from Figure 9(b), the trend of actual measured monostatic RCS is basically consistent with simulated result. Because the size of anechoic chamber is limited, the wave emitted from the horn is basically spherical wave when it

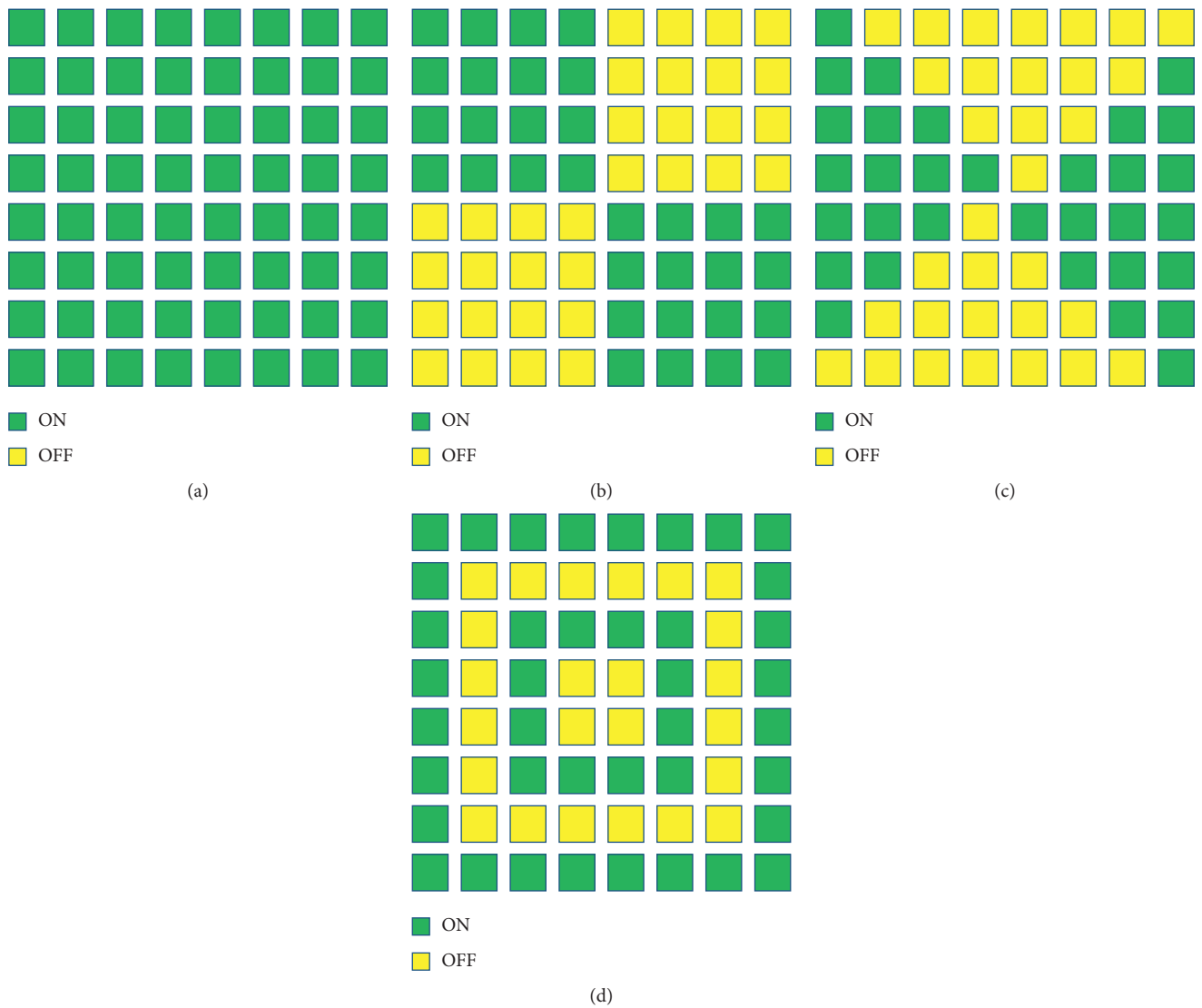


FIGURE 5: Simple version diagram of different layouts; (a) reference antenna (when all PIN diodes are of “ON” or “OFF” states, here just take all “ON” states as an example); (b) checkerboard layout; (c) new chessboard layout; (d) “0101” square ring nested layout.

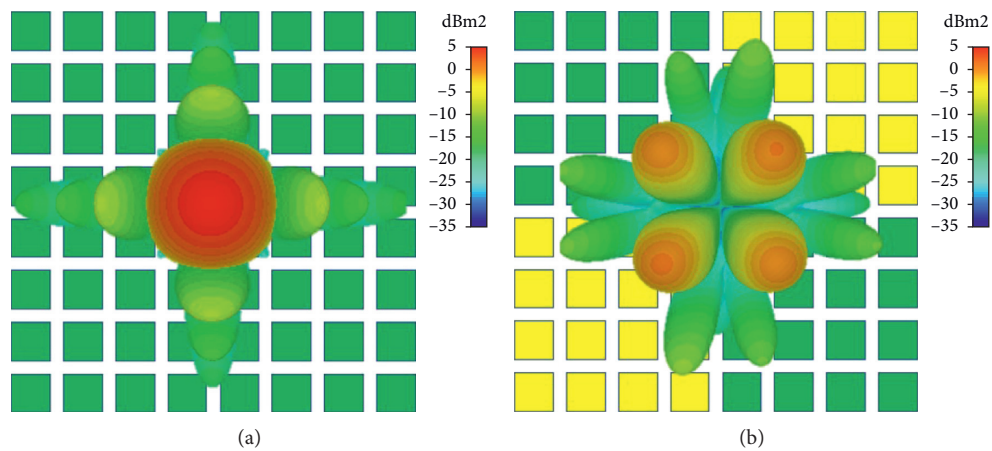


FIGURE 6: Continued.

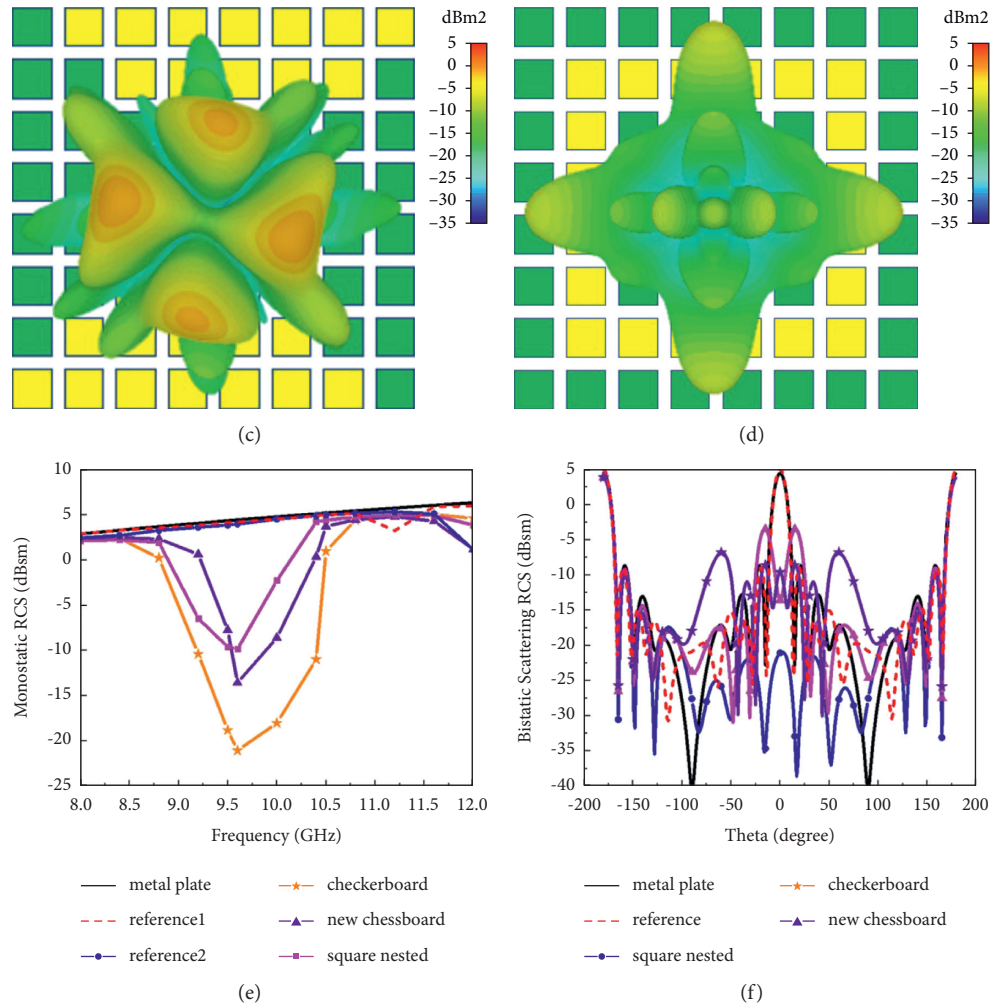


FIGURE 6: Simulated scattering results of different layouts; (a) reference antenna (when all PIN diodes are of “ON” or “OFF” states, here just take all “ON” states as an example); (b) checkerboard layout; (c) new chessboard layout; (d) “0101” square ring nested layout; (e) monostatic RCS variation curves with frequency; (f) bistatic RCS changing curves with angle.

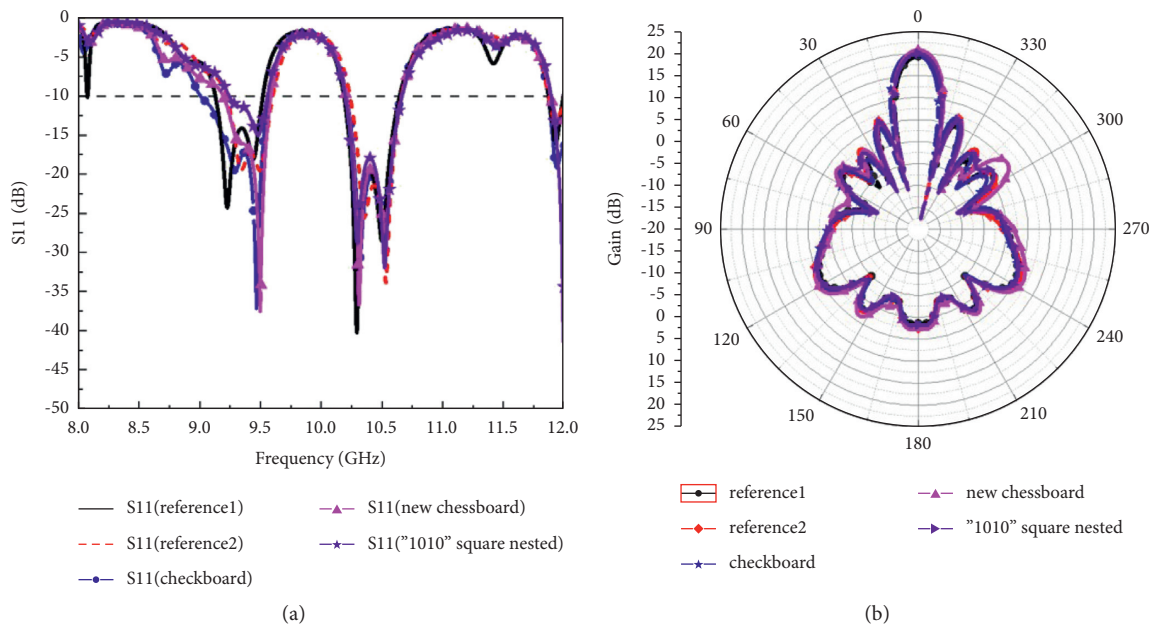


FIGURE 7: Simulated radiation results of different layouts; (a) amplitude of reflection of various structures; (b) comparison between realized gains of different layouts.

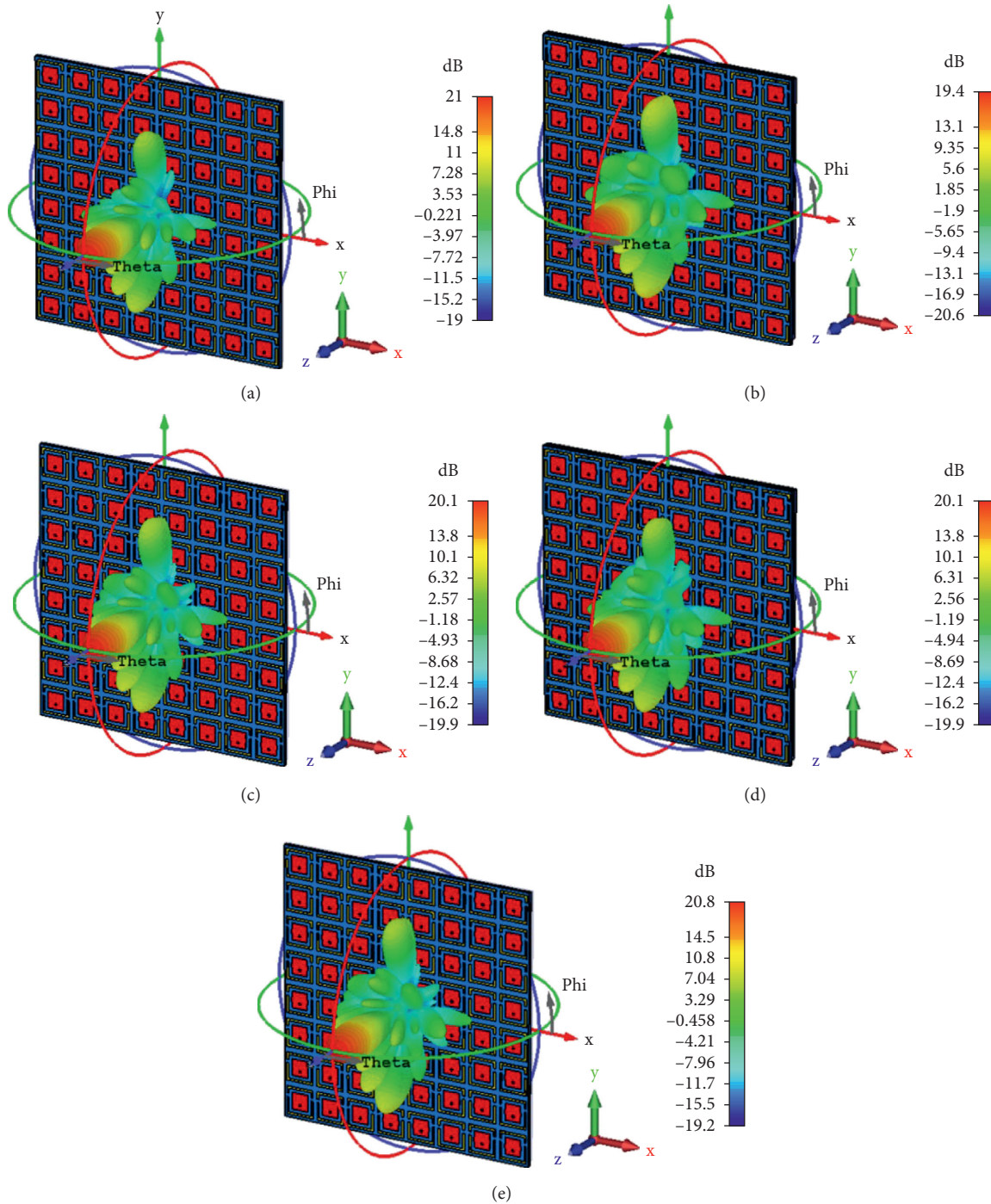
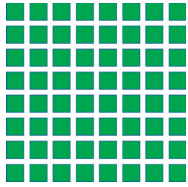
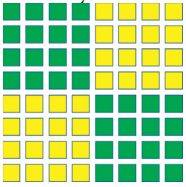
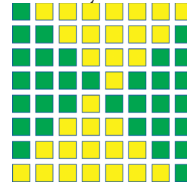
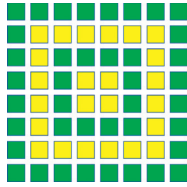


FIGURE 8: Simulated 3D radiation pattern of different layouts; (a) 3D radiation pattern of reference antenna (when all PIN diodes are of “ON” states); (b) 3D radiation pattern of reference antenna (when all PIN diodes are of “OFF” states); (c) 3D radiation pattern of checkerboard layout; (d) 3D radiation pattern of new chessboard layout; (e) 3D radiation pattern of “0101” square ring nested layout.

irradiates the surface of the object. This cannot fully reach the excitation condition of plane wave. In addition, the accuracy error during actual processing and the on-site environmental noise which is difficult to be eliminated (such as target holder used to support the sample and rotating platform) also result in a certain error between the actual measurement and the simulation result. But in general, the measured results can still prove that it has a good stealth effect. From Figure 10(b), there

is 300 MHz deviation between the measured frequency band and the simulation value. The main reason for the frequency offset is that in the actual processing, the triple-layer dielectric plates are mainly connected by metal vias. There will inevitably be a little air layer in the gap, which causes the frequency deviation. The measured gain of antenna in Figure 10(c) at frequency point 9.6 GHz is 17.8 dB, which is 1.1 dB lower than simulated result, and the measured gain of antenna in

TABLE 1: Basic performance comparison of three different layout antennas and reference antenna.

	Reference antenna	Checkerboard layout	New chessboard layout	“0101” square ring nested layout
				
6 dBsm RCS reduction bandwidth	—	8.7–10.5 GHz 18.8%	9.2–10.5 GHz 13.2%	9.0–10.2 GHz 12.5%
Maximum reduction of RCS at the scattering resonance point	—	21.0 dBsm 9.5 GHz	19.8 dBsm 9.5 GHz	15.0 dBsm 9.5 GHz
Strong scattering beam angle	$\theta = 0^\circ$	$\varphi = 45^\circ, \theta = \pm 45^\circ$ $\varphi = -45^\circ, \theta = \pm 45^\circ$	$\varphi = 0^\circ, \theta = \pm 45^\circ$ $\varphi = 90^\circ, \theta = \pm 45^\circ$	$\varphi = 0^\circ, \theta = \pm 16^\circ, \pm 35^\circ, \pm 60^\circ$ $\varphi = 90^\circ, \theta = \pm 17^\circ, \pm 38^\circ, \pm 60^\circ$

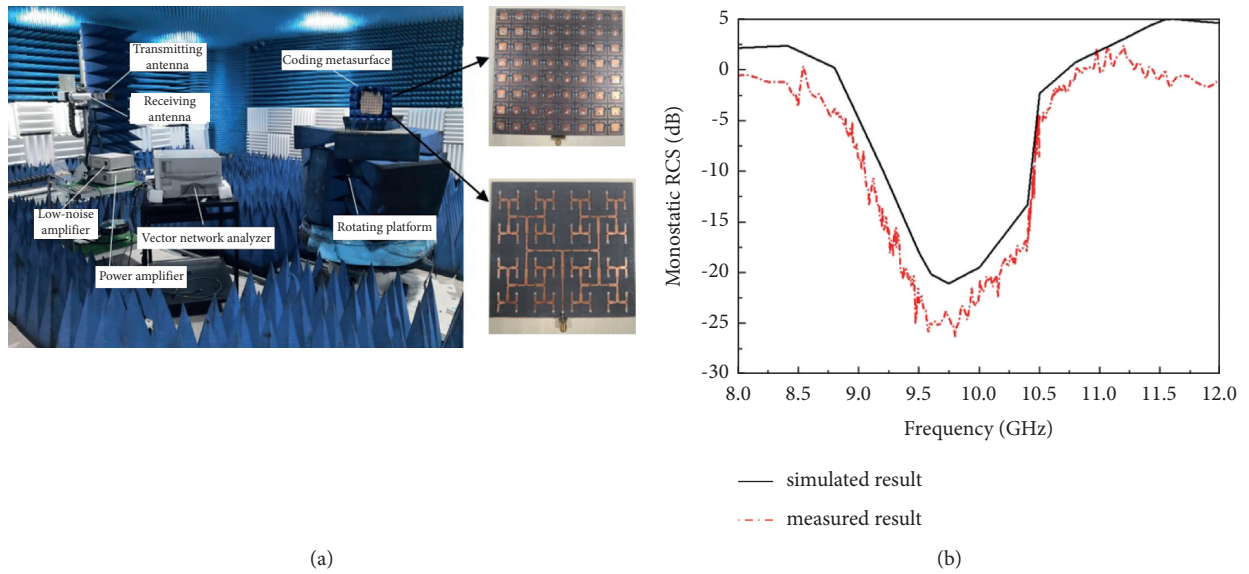


FIGURE 9: Measured scattering performance; (a) RCS measured environment; (b) measured monostatic RCS results.

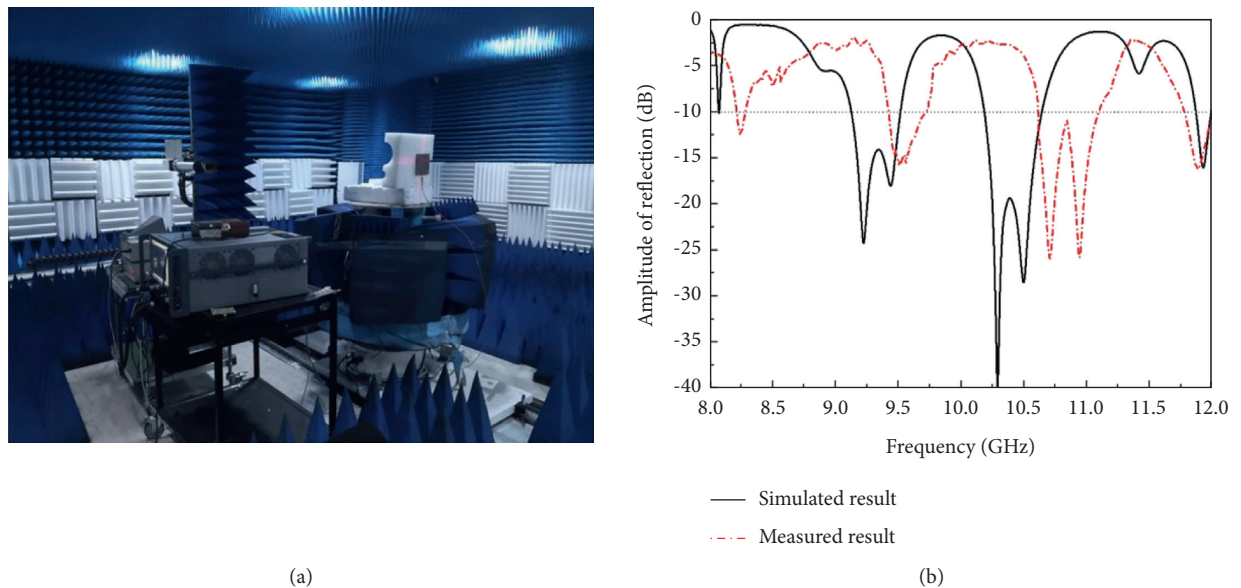


FIGURE 10: Continued.

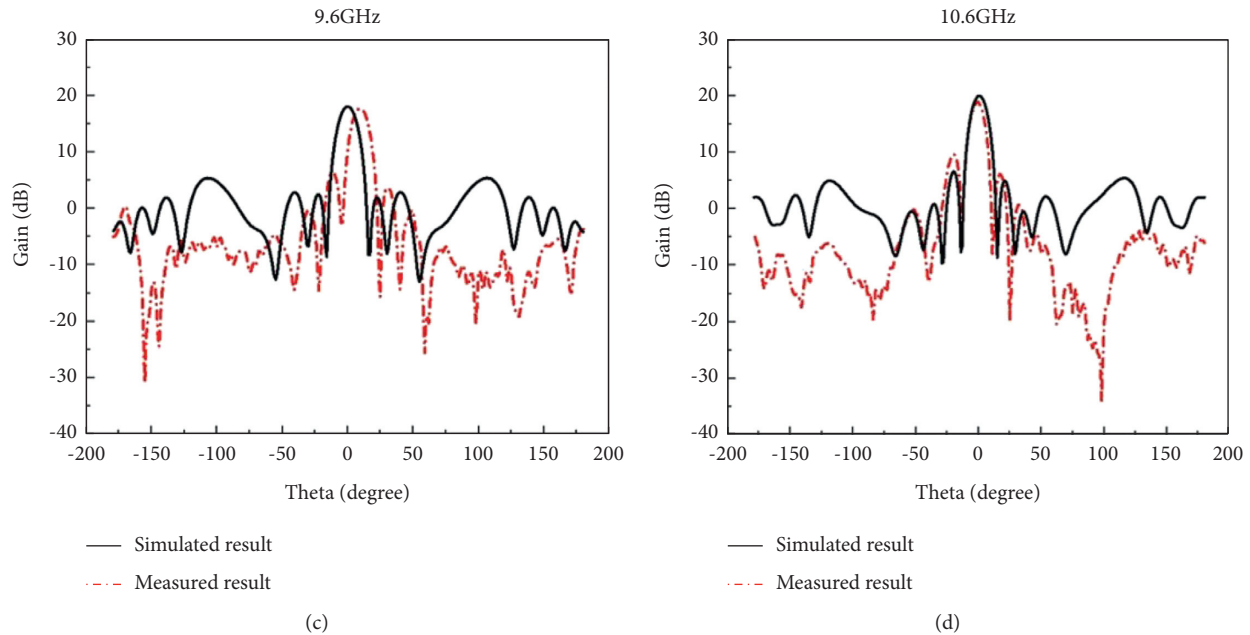


FIGURE 10: Measured radiation property; (a) radiation performance measured environment; (b) measured S11; (c) comparison between measured and simulated gain at 9.6 GHz; (d) comparison between measured and simulated gain at 10.6 GHz.

Figure 10(d) at frequency point 10.6 GHz is 20.4 dB, which is 0.6 dB lower than simulated result. This deviation can be attributed to the loss of the air layer and the losses of PIN diodes. Anyway measured results also prove that the radiation performance of this structure is almost unaffected.

4. Conclusion

To sum up, we have proposed a coding metasurface antenna array which possesses various reconfigurable scattering patterns. Both simulated and measured results demonstrate the feasibility of this structure since an ideal RCS reduction effect can be achieved no matter the structure is of checkerboard layout, new chessboard layout, or “0101” square ring nested layout while antenna radiation performance almost unaffected. This work may pave the way for antenna stealth technology, which has great potential for future changeable battlefield.

Data Availability

No data were used to support this study.

Conflicts of Interest

The authors declare that they have no conflicts of interest.

References

- [1] W. Ying Liu, Y. Tao Hong, S. Gong, and T. Hong, “Application of bionics in antenna radar cross section reduction,” *IEEE Antennas and Wireless Propagation Letters*, vol. 8, pp. 1275–1278, 2009.
- [2] C. M. Dikmen, S. Cakir, and G. C. akır, “Planar octagonal-shaped UWB antenna with reduced radar cross section,” *IEEE Transactions on Antennas and Propagation*, vol. 62, no. 6, pp. 2946–2953, 2014.
- [3] J. Xue, W. Jiang, and S. Gong, “Wideband rcs reduction of microstrip antenna based on 2.5-dimension miniaturized frequency selective surface,” in *Proceedings of the IEEE 5th Asia-Pacific Conference on Antennas and Propagation (AP-CAP)*, pp. 209–210, IEEE, Kaohsiung, Taiwan, July 2016.
- [4] S. Genovesi, F. Costa, and A. Monorchio, “Low-profile array with reduced radar cross section by using hybrid frequency selective surfaces,” *IEEE Transactions on Antennas and Propagation*, vol. 60, no. 5, pp. 2327–2335, 2012.
- [5] X. Huang, G. Wan, N. Wang, and X. Ma, “Radar cross section microstrip antenna based on slotted frequency selective surface,” *Microwave and Optical Technology Letters*, vol. 62, no. 10, pp. 3283–3291, 2020.
- [6] S. Lu, J. Huang, L. Song, and M. Yi, “A study on zoning coating method of absorbing materials for stealth aircraft,” *Optik*, vol. 208, Article ID 163912, 2020.
- [7] A. Kumar and S. Singh, “Development of coating for radar absorbing materials at X-band,” *IOP Conference Series: Materials Science and Engineering*, vol. 330, Article ID 12006, 2018.
- [8] Y. Zheng, J. Gao, X. Cao, Z. Yuan, and H. Yang, “Wideband RCS reduction of a microstrip antenna using artificial magnetic conductor structures,” *IEEE Antennas and Wireless Propagation Letters*, vol. 14, pp. 1582–1585, 2015.
- [9] Y. Liu, Y. Hao, K. Li, and S. Gong, “Radar cross section reduction of a microstrip antenna based on polarization conversion metamaterial,” *IEEE Antennas and Wireless Propagation Letters*, vol. 15, pp. 80–83, 2016.
- [10] Z. Yu and G. Z. Lu, “Ultra-broadband metamaterial absorber using slotted metal loops with multi-layers and its ecm analysis,” in *Proceedings of the IEEE 6th International Symposium on Microwave, Antenna, Propagation, and EMC Technologies (MAPE)*, pp. 426–428, IEEE, Shanghai, China, October 2015.
- [11] Q. Chen, S. Bie, W. Yuan, Y. Xu, H. Xu, and J. Jiang, “Low frequency absorption properties of a thin metamaterial

- absorber with cross-array on the surface of a magnetic substrate,” *Journal of Physics D: Applied Physics*, vol. 49, no. 42, Article ID 425102, 2016.
- [12] W. X. Jiang and X. G. Zhang, “Digital metasurfaces controlled by light, 2019,” in *Proceedings of the International Applied Computational Electromagnetics Society Symposium (ACES)*, vol. 1-2, IEEE, Miami, FL, USA, April 2019.
- [13] S. Iqbal, S. Liu, R. Y. Wu, G. D. Bai, Q. Ma, and T. J. Cui, “Polarization-selective dual-band digital coding metasurface for controls of transmitted waves,” *Journal of Physics D: Applied Physics*, vol. 51, no. 28, Article ID 285103, 2018.
- [14] L. Bao, Q. Ma, G. Bai, H. Jing, R. Wu, and X. Fu, “Design of digital coding metasurfaces with independent controls of phase and amplitude responses,” *Applied Physics Letters*, vol. 113, Article ID 63502, 2018.
- [15] L. Zhang, X. Wan, S. Liu et al., “Realization of low scattering for a high-gain fabry-perot antenna using coding metasurface,” *IEEE Transactions on Antennas and Propagation*, vol. 65, no. 7, pp. 3374–3383, 2017.
- [16] L. Zhang, R. Y. Wu, G. D. Bai et al., “Transmission-reflection-integrated multifunctional coding metasurface for full-space controls of electromagnetic waves,” *Advanced Functional Materials*, vol. 28, no. 33, Article ID 1802205, 2018.
- [17] H. Wang, L. Deng, C. Zhang, M. Qu, L. Wang, and S. Li, “Dual-band reconfigurable coding metasurfaces hybridized with vanadium dioxide for wavefront manipulation at terahertz frequencies,” *Microwave and Optical Technology Letters*, vol. 61, no. 12, pp. 2847–2853, 2019.
- [18] Z. Liang, J. Ouyang, and F. Yang, “-layer metasurface antenna,” *Electronics Letters*, vol. 54, no. 24, pp. 1362–1364, 2018.
- [19] Q. Cao, C. Meng, and J. Shi, “A triple-slotted substrate integrated cavity-fed 2x2 metasurface antenna with wide bandwidth,” *International Journal of RF and Microwave Computer-Aided Engineering*, vol. 29, 2019.
- [20] R. Swain, D. K. Naik, and A. K. Panda, “Low-loss ultra-wideband beam switching metasurface antenna in X-band,” *IET Microwaves, Antennas & Propagation*, vol. 14, no. 11, pp. 1216–1221, 2020.
- [21] W. E. I. Liu, Z. N. Chen, X. Qing, J. Shi, and F. H. Lin, “Miniaturized wideband metasurface antennas,” *IEEE Transactions on Antennas and Propagation*, vol. 65, no. 12, pp. 7345–7349, 2017.
- [22] Y. Fan, J. Wang, Y. Li, J. Zhang, Y. Han, and S. Qu, “Low-RCS and high-gain circularly polarized metasurface antenna,” *IEEE Transactions on Antennas and Propagation*, vol. 67, no. 12, pp. 7197–7203, 2019.
- [23] Y. Liu, Y. Jia, W. Zhang, Y. Wang, S. Gong, and G. Liao, “An integrated radiation and scattering performance design method of low-RCS patch antenna array with different antenna elements,” *IEEE Transactions on Antennas and Propagation*, vol. 67, no. 9, pp. 6199–6204, 2019.
- [24] A. Y. Modi, C. A. Balanis, C. R. Birtcher, and H. N. Shaman, “New class of RCS-reduction metasurfaces based on scattering cancellation using array theory,” *IEEE Transactions on Antennas and Propagation*, vol. 67, no. 1, pp. 298–308, 2019.